Order Parameters of a Transmembrane Helix in a Fluid Bilayer: Case Study of a WALP Peptide

Andrea Holt,[¶△] Léa Rougier,[†‡§△] Valérie Réat,[†§] Franck Jolibois,[‡§] Olivier Saurel,[†§] Jerzy Czaplicki,[†§] J. Antoinette Killian,[¶] and Alain Milon[†§*]

[†]Université de Toulouse-Université Paul Sabatier, IPBS, Toulouse, France; [‡]Université de Toulouse-Institut National des Sciences Appliquées-Université Paul Sabatier, LPCNO, Toulouse France; [§]Centre National de la Recherche Scientifique, Toulouse, France; and [¶]Utrecht University, Biochemistry of Membranes, Bijvoet Center for Biomolecular Research, Utrecht, The Netherlands

ABSTRACT A new solid-state NMR-based strategy is established for the precise and efficient analysis of orientation and dynamics of transmembrane peptides in fluid bilayers. For this purpose, several dynamically averaged anisotropic constraints, including ^{13}C and ^{15}N chemical shift anisotropies and ^{13}C-^{15}N dipolar couplings, were determined from two different triple-isotope-labeled WALP23 peptides (^{2}H, ^{13}C, and ^{15}N) and combined with previously published quadrupolar splittings of the same peptide. Chemical shift anisotropy tensor orientations were determined with quantum chemistry. The complete set of experimental constraints was analyzed using a generalized, four-parameter dynamic model of the peptide motion, including tilt and rotation angle and two associated order parameters. A tilt angle of 21° was determined for WALP23 in dimyristoylphosphatidylcholine, which is much larger than the tilt angle of 5.5° previously determined from ^{2}H NMR experiments. This approach provided a realistic value for the tilt angle of WALP23 peptide in the presence of hydrophobic mismatch, and can be applied to any transmembrane helical peptide. The influence of the experimental data set on the solution space is discussed, as are potential sources of error.

INTRODUCTION

In a number of recent publications, the orientation of transmembrane peptides has been discussed, particularly in the context of hydrophobic mismatch (1,2). The standard NMR method of probing the tilt and rotation angle of a peptide in a bilayer is based on the polarization inversion with spin exchange at magic angle (PISEMA (3)) experiment, which measures the ^{15}N chemical shift and ^{15}N-H dipolar coupling on each amide bond. More recently, as an alternative approach, the geometric analysis of labeled alanines (GALA) was developed based on ^{2}H NMR quadrupolar splitting (4–6). With this method, relatively small tilt angles (typically 5–10°, 5.5° for WALP23 in 1,2-dimyristoyl-*sn*-glycero-3-phosphocholine (DMPC)), were determined for WALP peptides, which are model peptides designed as mimics of α-helical transmembrane segments of membrane proteins. In a recent study, ^{15}N PISEMA and ^{2}H GALA NMR approaches were compared on a similar peptide (GWALP23 in 1,2-dilauroylphosphatidylcholine), yielding in both cases a fairly small tilt angle of ~13–10° (7). Similar angle values were obtained by oriented circular dichroism (CD) (8) and attenuated total reflection (ATR) Fourier transform infrared (9) spectroscopies. These results are in apparent contradiction with recent molecular dynamics (MD) simulations, which show that these transmembrane peptides are subject to large-amplitude whole-body motions and that they adopt large tilt angles of, e.g., 31° ± 12° for WLP23 (10) or 33.5° ± 9° (11) for WALP23 in DMPC. Although the authors of these MD simulations themselves point out some limitations, such as the length required to properly sample the peptide's behavior, the simulations clearly reveal that neglecting dynamical averaging in ^{2}H quadrupolar splitting interpretation leads to erroneous tilt angles. Therefore, an accurate analysis of the NMR data requires models that include dedicated peptide motions. It has been discussed already that dynamical averaging may be an important factor in the interpretation of PISEMA experiments (12,13). Simulations of quadrupolar splitting of deuterated alanines in a peptide helix reveal that dynamical averaging has an even more pronounced effect on the quadrupolar splittings. This is illustrated in Fig. 1.

Fig. 1 *b* shows that using the GALA approach (no wobbling, no oscillation), a larger tilt angle leads to a stronger variation of the quadrupolar splitting for various label positions. If oscillations about the long axis of the peptide are included in the simulations, these variations of the quadrupolar splitting are dampened. This behavior is illustrated in Fig. 1 *c* for a peptide with a tilt angle of 12° with $\Delta\rho$ varying from 1° to 150°. In such a way, averaging via oscillations gives rise to an apparent tilt angle smaller than its actual value. Finally, in Fig. 1 *d*, wobbling-in-a-cone motions around the helix axis are also included in the simulations, and it is shown that similar curves can be achieved for different sets of parameters.

From these simulations, it is obvious that quadrupolar splittings alone are not sufficient to distinguish various

Submitted September 29, 2009, and accepted for publication January 5, 2010.

△A. Holt and L. Rougier contributed equally to this work.

*Correspondence: alain.milon@ipbs.fr

A. Holt's present address is The Netherlands Cancer Institute, Amsterdam, The Netherlands.

Editor: William C. Wimley.

0006-3495/10/05/1864/9 $2.00

doi: 10.1016/j.bpj.2010.01.016

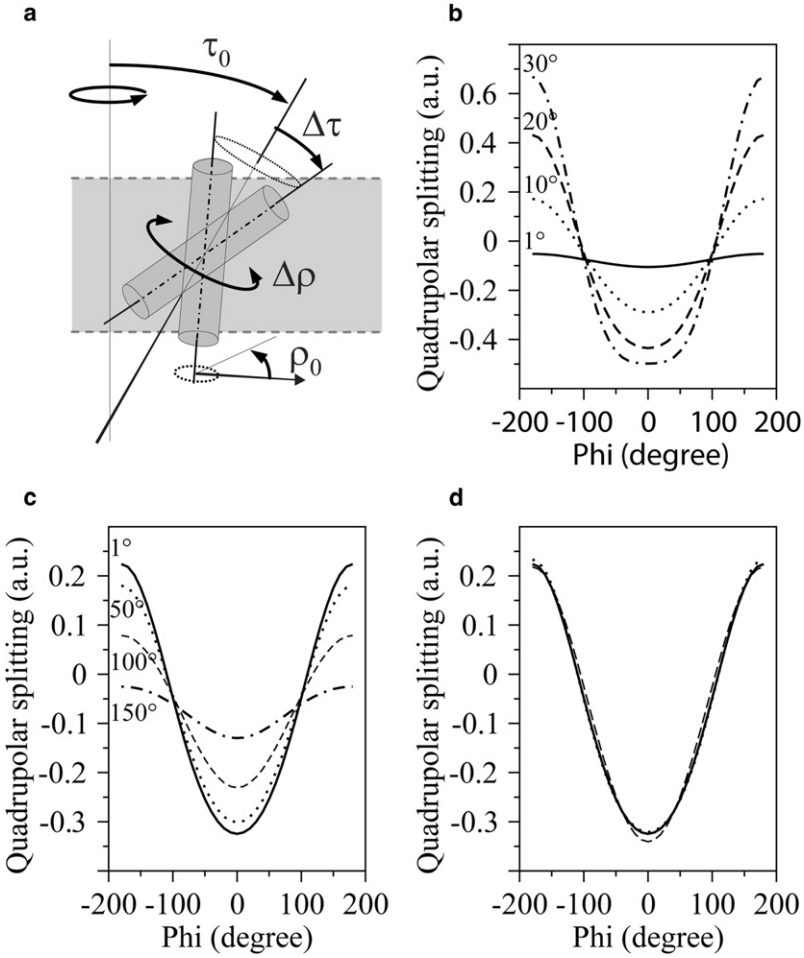

FIGURE 1 Influence of dynamical averaging on quadrupolar splitting. (*a*) Dynamic model describing the orientation and the dynamics of the peptide by a wobbling ($\Delta\tau$) in a cone around the averaged value of the helix tilt angle (τ_0) and an oscillations ($\Delta\rho$) around the averaged value of helix rotation angle (ρ_0). The fast axial diffusion takes place around the bilayer normal. (*b–d*) The three graphs represent the dependence of the quadrupolar splitting as a function of the label position around the helix (characterized by the ψ angle). (*b*) Variation for four tilt angles, τ_0 (1°, 10°, 20°, and 30°), with no wobbling and no oscillation. (*c*) Variation for a tilt angle of $\tau_0 = 12°$, with oscillations of $\Delta\rho = 1°$, 50°, 100°, and 150°. (*d*) Comparison of three dynamical models, ($\tau_0 = 12°$, $\Delta\tau = 0°$, $\Delta\rho = 0°$), ($\tau_0 = 6°$, $\Delta\tau = 10°$, $\Delta\rho = 0°$), and ($\tau_0 = 18°$, $\Delta\tau = 0°$, $\Delta\rho = 80°$). All plots were obtained for the same value of helix rotation angle (ρ_0).

dynamical models as soon as wobbling and oscillations are taken into account, and that neglecting such peptide motions can lead to an underestimation of the tilt angle (such as 12° instead of 18°). Similar behavior was described recently in a study by Strandberg et al. (13). It is therefore essential to add different experimental anisotropic interactions (such as chemical shift anisotropy and dipolar coupling) when performing a dynamical analysis. The recent work of Vostrikov et al. (7) is along this line, combining ^{2}H NMR and PISEMA experiments. However, the data were analyzed with a semistatic, two-parameter model, with the associated artifacts illustrated above (the term semistatic is employed since a global, isotropic order parameter, scaling down the NMR interaction, is often included).

In this study, we establish an approach based on complementary anisotropic constraints to analyze the dynamics of membrane peptides, which to our knowledge is a new approach. For this purpose, two triple-isotope-labeled WALP peptides have been synthesized. Additional anisotropic NMR parameters, including two ^{15}N amide chemical shift anisotropies (CSAs), two ^{13}C carbonyl CSAs, and two ^{15}N-^{13}C dipolar couplings (DCs) between spins connected via the peptide bond were determined and combined with the six previously determined alanine methyl ^{2}H quadrupolar splittings (6). The previous deuterium NMR data already showed that the peptide is tilted (i.e., that its most probable orientation is not the bilayer normal) and that fast axial diffusion is active along the bilayer normal but not along the α-helix axis (the bilayer normal is an axis of symmetry for the movement, the α-helix axis is not). Therefore, a simple Maier-Saupe orienting potential (14) cannot be used to describe the peptide motion. The data analysis is thus based on a helix rigid-body motion characterized by (see Fig. 1 *a*): 1), a fast axial diffusion of the peptide around the bilayer normal; 2), an averaged position of the peptide in the bilayer defined by a tilt angle, τ_0 (between the diffusion axis and the α-helix axis), and a rotation angle, ρ_0 (around the α-helix axis); 3), a wobbling amplitude, $\Delta\tau$, around the averaged tilt angle, τ_0; and 4), an oscillation amplitude, $\Delta\rho$, around the averaged rotation angle, ρ_0.

The anisotropic NMR interactions each explore a large range of orientations of the principal axis system (PAS) with respect to the helix axis, with the ^{15}N CSA being mostly sensitive to tilt and wobbling (as in the PISEMA approach), whereas the other anisotropic constraints are sensitive to a combination of the four parameters, each in a specific way.

This appears to be essential for the identification of a unique motional model capable of fitting all the experimental data.

MATERIALS AND METHODS

Materials

DMPC was obtained from Avanti Polar Lipids (Alabaster, AL) and used without further purification. Two different ^{2}H, ^{13}C, and ^{15}N isotopically labeled WALP23 peptides (acetyl-GW2(LA)8LW2A-NH2) were synthesized using Fmoc/tBu solid-phase synthesis, WALP23($^2H_3$-Ala^{13}, $^{13}C_1$-Ala^{11},^{15}N-Leu^{12}), referred to as WALP23#1, and WALP23($^2H_3$-Ala^7, $^{13}C_1$-Ala^{13},^{15}N-Leu^{14}), referred to as WALP23#2. Deuterium-labeled L-alanine (3,3,3-d_3, 99%), $^{13}C_1$-labeled L-alanine (1-^{13}C, 99%), and ^{15}N-labeled L-leucine (^{15}N, 98%) were purchased from Cambridge Isotope Laboratories (Andover, MA). Fmoc (9-fluorenylmethyloxycarbonyl) was used to protect its amino functionality, as described by ten Kortenaar et al. (15), before being used in the peptide synthesis. The molecular mass of the synthesized peptides was verified by mass spectrometry and the purity was analyzed by high-performance liquid chromatography (HPLC) using a C4 reverse-phase HPLC column. For analytical and, if necessary, preparative HPLC, a solvent system with solvent A, composed of 95% water, 5% acetonitrile, and 0.1% TFA (trifluoroacetic acid), and solvent B, composed of 80% acetonitrile, 20% isopropanol, and 0.1% TFA, was used. The purity of the peptides used in this study was >95%.

NMR sample preparation

Static parameters of ^{15}N and ^{13}C anisotropic interactions were determined from lyophilyzed WALP23 peptide, and 6.5 μmol of powder of each peptide were packed into a 3.2-mm rotor. The ^{2}H static quadrupolar coupling constant of Ala methyl was measured on 60 mg of dry WALP23#2 peptide. For WALP23 inserted into large unilamellar vesicles of DMPC, solutions of 20 mM DMPC in chloroform were prepared, and the lipid concentration was determined by the Rouser phosphorus assay. Solutions of WALP23 were prepared with a concentration of 500 μM in trifluoroethanol and the concentration of WALP23 was determined by absorption spectroscopy using an extinction coefficient of 22,400 M^{-1} cm^{-1} at 280 nm. Unoriented samples, i.e., liposomes, were used instead of oriented bilayers to allow complete control of the hydration level. Typically, 0.7 μmol of WALP23 peptides and 70 μmol DMPC were mixed in solution (1:100 peptide/lipid molar ratio). The organic solvents were evaporated under a nitrogen flow and further removed under vacuum overnight (ca. 10^{-2} mbar). Subsequently, the samples were hydrated with Milli-Q water and lyophilized to yield a fluffy powder, facilitating a thorough hydration at the low hydration levels needed. The unoriented samples were hydrated with deuterium-depleted water to 33% (water/(water + lipid + peptide), w/w) and incubated overnight at 37°C to equilibrate the hydration throughout the sample.

NMR experiments

Solid-state magic angle spinning (MAS) experiments were carried out on a Bruker (Billerica, MA) Avance narrow-bore spectrometer operating at 700.13 MHz for ^{1}H. A Bruker 3.2-mm MAS triple-tuned solenoid coil was used for ^{13}C and ^{15}N experiments. Nonspinning ^{2}H and ^{15}N spectra were recorded on a Bruker Avance narrow-bore spectrometer operating at 500.13 MHz for ^{1}H with a 5-mm simple-resonance and a 7-mm double-resonance probe, respectively, both equipped with a solenoid coil oriented at 90° with respect to the magnetic field. The sample temperature was 313 K in every case. ^{13}C spectra were referenced to 2,2-dimethyl-2-silapentane-5-sulphonate and ^{15}N spectra to liquid ammonia, using the ^{1}H chemical shift of lipid's methyl resonances (0.85 ppm) as an internal reference for each nucleus.

^{13}C and ^{15}N static and averaged CSA parameters were determined from standard cross-polarization (CP) MAS spectra. Isotropic chemical shifts were determined at a spinning frequency of 10 kHz. CSAs were recorded by spinning side-band analyses. Typically, 4 kHz and 3 KHz, respectively, were used for the ^{13}C and ^{15}N static CSA determinations, whereas 0.75 kHz and 1kHz were used for the averaged CSA of WALP23 peptides into DMPC liposomes. ^{15}N CSA of WALP in lipid bilayers was also determined from the static NMR powder spectrum. ^{13}C-^{15}N dipolar couplings were determined using a standard REDOR (16) experiment at a spinning frequency of 10 kHz, the $\Delta S/S_0$ REDOR curves were fitted in a standard manner (17) using Mathcad software (17–19). Deuterium NMR spectra were acquired using a standard quadrupolar echo pulse sequence (see Supporting Material for details on NMR experiments).

Determination of experimental static and dynamically averaged CSA

^{13}C CSA parameters were obtained by the analysis of spinning side-band intensity using Dmfit freeware (http://crmht-europe.cnrs-orleans.fr/dmfit/).The static CSA and the asymmetry parameter were defined as $\delta_{aniso} = \delta_{33} - \delta_{iso}$ and $\eta = (\delta_{22} - \delta_{11})/(\delta_{33} - \delta_{iso})$, respectively, with $|\delta_{33} - \delta_{iso}| \geq |\delta_{11} - \delta_{iso}| \geq |\delta_{22} - \delta_{iso}|$. The ^{13}C averaged CSA values were determined by using a Hertzfeld-Berger analysis to extract the components of the ^{13}C dynamically averaged axially symmetric CSA, defined as $CSA_{exp} = 3/2\ (\delta_{90°} - \delta_{iso})$, where $\delta_{90°}$ is the chemical shift of peptide in membrane oriented at 90° with respect to the magnetic field and δ_{iso} is the isotropic chemical shift. ^{15}N averaged axially symmetric CSA_{exp} values were determined from $\delta_{90°}$ and δ_{iso}, respectively, measured on a powder static ^{15}N spectrum and on a CP-MAS spectrum at 10 kHz of spinning frequency (6).

Quantum chemistry calculation

The peptide's geometry and the ^{15}N and ^{13}C CSA static tensor components (more specifically, principal axis orientation with respect to the helix geometry) are required for the calculation of dynamically averaged anisotropic interactions. Both the structure and the static theoretical NMR spectroscopic data were determined using a quantum chemical approach.

All quantum chemical calculations were performed using the Gaussian 03 suite of programs (20). Molecular geometries of WALP23 were optimized starting from a perfect canonical α-helix structure ($\Phi = -58°$ and $\Psi = -47°$) using the ONIOM hybrid approach (21,22) that divides the system into an active and an inactive part. The active part (seven residues centered on the Ala^{11}-Leu^{12} or the Ala^{13}-Leu^{14} peptide bond) was calculated using the hybrid density functional theory B3LYP method (23,24) associated with a Pople-type double ξ basis set augmented by polarization functions on all atoms (namely, 6-31G(d,p)) (25). The inactive part of the system (the rest of the peptide) was calculated using a semiempirical (AM1) approach (26–28). NMR chemical shielding tensors were computed at the B3LYP/6-31G(d,p) level of theory on the whole peptide using the gauge including atomic orbital method for the numerous advantages it offers (29–33).

To allow the calculation of motionally averaged CSA parameters, the molecular frame (M) was chosen as follows: the z axis is the main inertia axis of the α-helix; the x axis is perpendicular to the z axis and contains the Leu_{12} α-carbon; the y axis completes the direct orthonormal frame. Thus, α_{PM}^{CSA}, β_{PM}^{CSA}, and γ_{PM}^{CSA} (see Table 2 and Results and Discussion) are the Euler angles associated with the rotation matrix between the CSA tensor principal axis system PAS and the molecular frame M using the zyz convention. ^{15}N-$^{13}C_1$ dipolar-coupling and methyl Ala ^{2}H quadrupolar-coupling tensor orientations are defined by the spherical coordinates (Θ and Φ) of the ^{13}C-^{15}N and C_α-C_β bond in the molecular frame. The associated numerical values were extracted from the quantum chemical optimized geometries.

Computation of the dynamically averaged anisotropic interactions and experimental fittings

Using the static anisotropic tensor information obtained as described above, dynamically averaged interactions were computed using a four-parameter

model of motion involving tilt (τ_0), wobbling in a cone of angle ($\Delta\tau$), rotation (ρ_0), and oscillation of amplitude ($\Delta\rho$) (see Fig. 1 *a*). Internal dynamics of the peptide's helical structure, although certainly present, were assumed to be negligible based on the observation by molecular dynamics that the helical structure is well preserved during the simulations (11).

Both quadrupolar and dipolar splittings were computed from the expression

$$g\left(\beta_{PN}^{QC/DC}\right) = K_{QC/DC} \times \frac{3\cos^2\beta_{PN}^{QC/DC} - 1}{2},$$

where the constant $K_{QC/DC}$ depends on the type of interaction, quadrupolar (QC) or dipolar coupling (DC), respectively; $\beta_{PN}^{QC/DC}$ defines the orientation of the bilayer normal, *N*, relative to the principal axis frame of dipolar or quadrupolar interaction tensor (where the C-D quadrupolar tensor is quasiaxially symmetric). This equation is given for bilayers oriented with the bilayer normal parallel to the magnetic field.

The CSA effects depend on the spherical coordinates β_{PN}^{CSA} and α_{PN}^{CSA} of the bilayer normal $\vec{N}$ in the principal axis frame (PAF) of the CSA tensor (where η is the asymmetry parameter):

$$h\left(\beta_{PN}^{CSA}, \alpha_{PN}^{CSA}\right) = -K'_{CSA} \times \left[\left(\frac{3\cos^2\beta_{PN}^{CSA} - 1}{2}\right) - \frac{1}{2}\eta\left(\sin^2\beta_{PN}^{CSA}\cos 2\alpha_{PN}^{CSA}\right)\right].$$

Following the Wigner rotation matrix formalism (34), equations $g(\beta_{PN}^{QC/DC})$ and $h(\beta_{PN}^{CSA}, \alpha_{PN}^{CSA})$ were expressed as functions of the PAS orientation relative to the molecular frame (denoted *M*) and *M* orientation relative to the diffusion frame (denoted *N*).

Peptide motion in the submicrosecond timescale leads to time-modulated β_{PN}^{i} and α_{PN}^{i} angles, and was included by integrating $g(\beta_{PN}^{QC/DC})$ and $h(\beta_{PN}^{CSA}, \alpha_{PN}^{CSA})$ over the angles describing the movements, i.e., a variation of τ between $\tau_0 - \Delta\tau$ and $\tau_0 + \Delta\tau$ and of ρ between $\rho_0 - \Delta\rho$ and $\rho_0 + \Delta\rho$, as described in the Supporting Material.

The dynamically averaged theoretical anisotropic interactions (QCs, DCs, and CSAs) were then calculated and compared to the experimental data. The sum of their squared differences was minimized to obtain the best fit. To avoid the traps of local minima typical for gradient-based approaches, we have used GOSA (35), a multivariate global optimization program based on simulated annealing (http://www.bio-log.biz). To estimate errors of the best-fit parameters, a Monte Carlo approach was employed (36). A set of 100 combinations of experimental values was randomly generated within the limits of experimental error, and the fit was performed for each of them. This gave a representation of multiple minima in the four-parameter space (see, e.g., rows F1 and F2 in Table 3), and the range of possible values for each fitted parameter. Multidimensional integration was performed with the CUBA library (37).

RESULTS AND DISCUSSION

Secondary structure and aggregation state of WALP23

For interpretation of the solid-state NMR data in terms of a structural and dynamic model of WALP23, it first is important to know whether under the experimental conditions used, the peptide can be considered as a monomeric and stable helix, diffusing freely in the fluid bilayer.

Different studies have shown the backbone structure of the WALP peptides to be remarkably robust, even withstanding considerable mismatch. This is most clear from FTIR measurements, which showed, at the amide I position of a range of different-length WALP peptides, an intense narrow band that did not shift or broaden upon either increasing or decreasing bilayer thickness (9). Also, CD measurements (9,38) showed an α-helical structure under a range of conditions, and fits of ^{2}H NMR data on Ala-d_4-labeled peptides suggested significant distortion only at conditions of extreme positive mismatch (39). In addition, a variety of MD simulations suggested a rather perfect and robust α-helix (11,40). With respect to the aggregational behavior, it should be mentioned that different lines of experimental evidence suggest that WALP23 by itself has no tendency to self-associate in a lipid bilayer. For example, the lipid flip-flop-promoting effect of the peptides was found to be perfectly linear over a wide range of peptide concentrations (41). Also, self-quenching of pyrene-labeled peptides was found to occur only at peptide concentrations significantly higher than those in this study (42), and the same holds for sucrose density gradient centrifugation experiments, which showed homogeneous peptide/lipid mixtures up to very high peptide/lipid ratios (38). So far, only in the gel phase of DPPC and other saturated lipids aggregates have been observed by AFM. However, these were linear aggregates, supporting in fact the notion that the peptides have a strong preference for interaction with lipids (43). Nevertheless, to avoid any risk of peptide aggregation, we performed our analysis on samples with a relatively low peptide/lipid ratio of 1:100.

Static ^{13}C and ^{15}N CSA tensor parameters computed by quantum chemistry

Static ^{13}C and ^{15}N CSAs and asymmetry parameters were found to be close to the experimental values obtained on dry peptide. Consequently, we can be confident of their correctness and, in particular, of the quality of the eigenvectors (tensor orientation relative to the molecular frame (see Table 1)). To check the accuracy of our theoretical chemical-shielding eigenvectors, we can define the tensor orientation relative to the peptide plane (Fig. 2 and Table 1).

For the ^{15}N tensor, α_N is the angle between e_{11} and the N^i-C^{i-1} peptide bond, β_N the angle between e_{22} and the normal to the peptide plane, and γ_N the angle between e_{33} and the N-H bond, where e_{ii} is the eigenvector associated with the σ_{ii} eigenvalue (see Fig. 3 for e_{ii} representation). For the $^{13}C_1$ tensor, α_C is the angle between e_{11} and the N^i-C^{i-1} peptide bond, β_C the angle between e_{22} and the

TABLE 1 Chemical shift tensor orientation relative to the peptide plane computed for WALP23 peptide

^{13}C	α_C	β_C	γ_C
Ala[11]	32.2	2.1	2.1
Ala[13]	31.8	2.4	2.0
^{15}N	α_N	β_N	γ_N
Leu[12]	20.9	17.9	19.2
Leu[14]	20.7	17.7	19.5

See text for details regarding definition of angles.

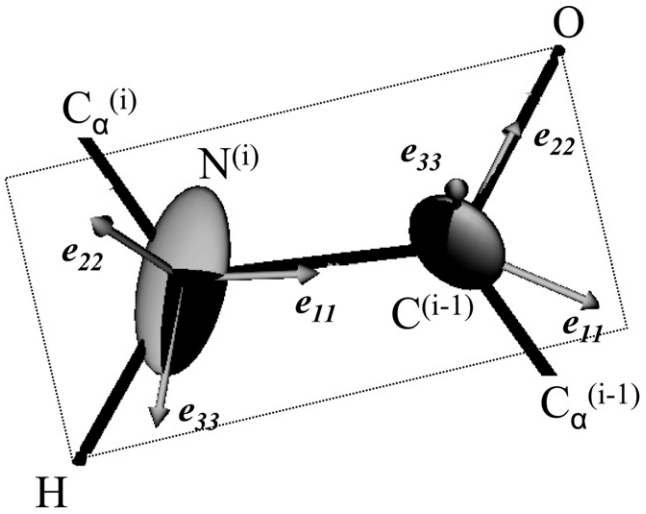

FIGURE 2 Schematic representation of eigenvector orientation with respect to the peptide plane for $^{13}C_1$ and ^{15}N CSA tensors.

C-O bond, and γ_C the angle between e_{33} and the normal to the peptide plane. The angles obtained on both peptides (see Table 1) are in agreement with the standard values used to describe ^{15}N and ^{13}C chemical-shift tensor eigenvectors (44–46). In particular, ^{15}N the angle between e_{33} and the N-H bond is equal to 19° and the e_{11} is tilted by ~21° from the peptide plane. For $^{13}C_1$, the α_C angle is close to 32°, e_{22} is almost colinear to the carbonyl C-O bond, and e_{33} is perpendicular to the peptide plane.

MAS NMR experiments on peptides inserted into membranes

To ensure compatibility of the existing ^2H NMR data with the new NMR data, a deuterium-labeled alanine was included in each peptide, which made it possible to check the sample conditions by deuterium NMR. For both triple-labeled peptides, the quadrupolar splittings found were identical to previously published values (6) (data not shown). In addition, each sample permitted the determination of the ^{15}N amide chemical shift and averaged CSA for one leucine, ^{13}C carbonyl chemical shift and averaged CSA for one alanine (Fig. 3), and one ^{15}N-^{13}C dipolar coupling linked to the dynamics and orientation of the N-C_1 peptide bond (data not shown).

Isotropic chemical shifts were determined at a spinning frequency of 10 kHz on both peptides inserted into bilayers. The carbonyl ^{13}C line widths were equal to 0.3 ppm, which is a good indication of structural homogeneity. The isotropic ^{13}C chemical shift, 178.9 ppm in both cases, was typical for a peptide in a helical conformation, confirming that the peptide's dynamics preserves a helical conformation at positions 11 and 13.

To determine dynamically averaged CSAs, two strategies were applied, depending on spectral overlap and sensitivity of each nucleus. For ^{13}C, dynamically averaged CSAs were obtained from slow-spinning side-band MAS spectral analysis, which makes it possible to resolve resonances arising from the peptides and those arising from natural-abundance lipid carbonyls (see Fig. 3 *a*). For ^{15}N dynamically averaged CSAs, the most efficient method, due to the low signal intensity, appeared to be a comparison between the isotropic chemical shift measured under MAS conditions and the powder spectrum measured under static conditions. The most intense shoulder of the powder spectrum provides a value of $\delta_{90°}$ (Fig. 3 *b*), as was already proposed by Cady et al. (47) for axially diffusing peptides. The magic-angle hole can be seen in ^{15}N static spectra and results from the colinearity of the chemical-shift tensor and the dipolar-coupling tensor in uniaxially mobile molecules (48).

The CSA values for both ^{15}N and ^{13}C confirm the dynamical behavior of the peptide, since they are significantly lower in liposomes than in peptide powder (compare, for

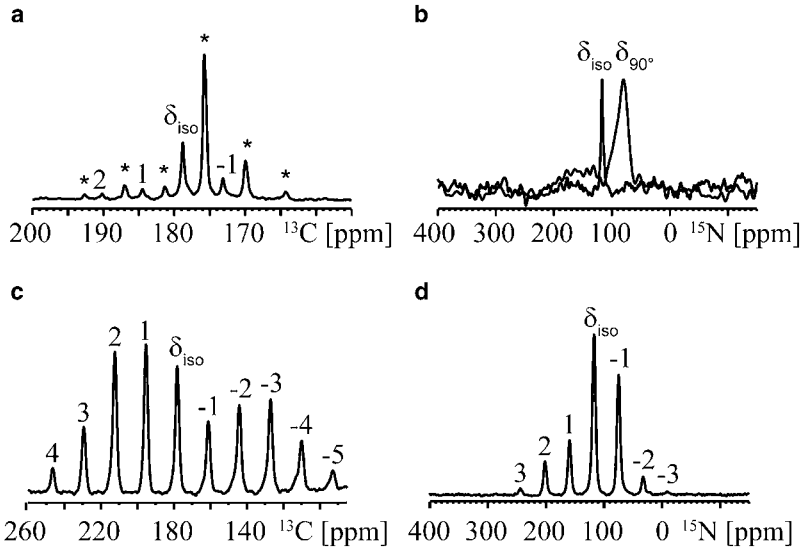

FIGURE 3 ^{13}C and ^{15}N MAS NMR spectra for CSA determination for WALP23($^2H_3$-Ala^{13},$^{13}C_1$-Ala^{11}, ^{15}N-Leu^{12}) peptide in DMPC liposomes (molar ratio 1:100, wt % water of 33%) and and as a dry peptide. (*a*) $^{13}C_1$-Ala^{11} spinning side-band spectrum measured at 1 kHz spinning frequency. The peaks labeled with stars correspond to signals from lipid carbonyls. (*b*) Overlay of ^{15}N-Leu^{12} 10 kHz spinning MAS NMR spectrum (*black*) and ^{15}N-Leu^{12} NMR powder spectrum (*gray*) of liposomes, displaying the highest intensity for bilayers oriented at 90°. Similar data were obtained for WALP23 ($^2H_3$-Ala^7,$^{13}C_1$-Ala^{13},^{15}N-Leu^{14}) peptide in DMPC liposomes (data not shown). (*c*) $^{13}C_1$-Ala^{11} spinning side-band spectrum at 4 kHz spinning frequency, on dry peptide. (*d*) ^{15}N-Leu^{12} spinning side-band spectrum measured at 3 kHz spinning frequency on dry peptide. Similar data were obtained for WALP23($^2H_3$-Ala^7, $^{13}C_1$-Ala^{13},^{15}N-Leu^{14}) peptide (data not shown).

TABLE 2 Tensor components of the interactions used in the fitting procedure and experimental NMR parameters reflecting the peptide's dynamical behavior

Chemical shift tensors

	δ_{aniso}* (ppm)	η*	$\alpha_{PM}^{CSA\dagger}$ (°)	$\beta_{PM}^{CSA\dagger}$ (°)	$\gamma_{PM}^{CSA\dagger}$ (°)	$CSA_{exp}^{\ddagger}$ (ppm)
[^{13}C]Ala^{11}	−84.2	0.59	−82.0	97.7	323.3	−16.4 ± 1.6
[^{13}C]Ala^{13}	−85.1	0.62	−77.9	102.7	135.8	−20.1 ± 2.0
[^{15}N]Leu^{12}	104.6	0.20	−163.3	15.1	20.5	−105.6 ± 5.0
[^{15}N]Leu^{14}	104.5	0.19	−138.0	15.6	168.0	−114.6 ± 5.0

Dipolar interactions

	K* (Hz)	$\Theta^{\dagger}$ (°)	$\Phi^{\dagger}$ (°)	$DC_{exp}^{\ddagger}$ (Hz)
[^{13}C]Ala^{11}-[^{15}N]Leu^{12}	1010	68.9	312.4	313 ± 100
[^{13}C]Ala^{13}-[^{15}N]Leu^{14}	1010	69.3	114.6	286 ± 100

Quadrupolar interactions

	K* (Hz)	$\Theta^{\dagger}$ (°)	$\Phi^{\dagger}$ (°)	$\Delta\nu_Q^{\ddagger}$ (Hz)
CD_3-Ala^7	37,700	58.7	85.5	500 ± 500
CD_3-Ala^9	37,700	58.1	247.8	5725 ± 500
CD_3-Ala^{11}	37,700	58.7	50.3	1000 ± 500
CD_3-Ala^{13}	37,700	58.2	212.3	6025 ± 500
CD_3-Ala^{15}	37,700	58.6	15.0	500 ± 500
CD_3-Ala^{17}	37,700	58.3	176.9	6075 ± 500

*Experimental static values measured on dry peptides.
†Computed values.
‡Dynamically averaged values (measured on membrane-inserted peptide, at a wt % water of 33%). $CSA_{exp} = \delta_{90°} - \delta_{0°} = 3/2(\delta_{90°} - \delta_{iso})$ for peptide in axial diffusion around the lipid bilayer normal. $\delta_{aniso} = \delta_{33} - \delta_{iso}$, $\eta = (\delta_{22} - \delta_{11})/(\delta_{33} - \delta_{iso})$, with $|\delta_{33} - \delta_{iso}| \geq |\delta_{11} - \delta_{iso}| \geq |\delta_{22} - \delta_{iso}|$, $(\alpha_{PM}^i, \beta_{PM}^i, \gamma_{PM}^i)$ and (Θ, Φ) are the angles defining the CSA and dipolar or quadrupolar tensor orientations in the molecular frame (see Materials and Methods). Experimental uncertainties were estimated from two independent experiments and several sets of fitting parameters. They were not sensitive to line width, and the values finally retained and given in this table are very conservative (10% relative error in most cases, 5% for ^{15}N CSAs).

example, Fig. 3, *a* and *c*, and Fig. 3, *b* and *d*, and values in Table 2). Moreover, the asymmetry parameters extracted from spinning side-band analysis of the ^{13}C spectra were found to be null for both peptides in liposomes, in agreement with dynamics involving fast axial diffusion along the bilayer normal, as was already demonstrated in previous ^{2}H NMR experiments (5,6). The resulting part of the anisotropic interaction is directly related to the peptide's motion in terms of tilt (τ_0), rotation (ρ_0), wobbling ($\Delta\tau$), and oscillation ($\Delta\rho$).

All the computed static and experimentally determined static and dynamically averaged CSAs are summarized in Table 2, together with quadrupolar and dipolar splittings.

Data analysis and extraction of dynamical parameters

Six new anisotropic constraints have been determined, and these were combined with the previously published six quadrupolar splittings determined on peptides including deuterated alanines. As described in Materials and Methods, we then explored the entire space of possible solutions in terms of a four-parameter dynamical model involving tilt, τ_0, rotation, ρ_0, wobbling, $\Delta\tau$, and oscillations, $\Delta\rho$. In the fitting procedure, the principal axis orientations were taken from computed values, whereas the principal values were the experimental ones, measured on the dry peptide powder by standard spinning side-band analysis (see Table 2). The complementary orientations of the anisotropic tensors allowed for identification of a well-defined region of agreement between simulations and experiment, as illustrated in Fig. 4 and Table 3 (*line A*).

Several important conclusions can be drawn from this analysis:

1. The complete set of anisotropic constraints is sufficient to extract the complete orientation and dynamics of the WALP peptide in DMPC (Table 3, *line A*). The tilt and rotation angles are determined with good accuracy (20.8 ± 1.4° and 146 ± 7°, respectively), which agrees well with the tilt angle of 23° obtained recently using a fluorescence approach (49) and confirms the trends indicated in molecular dynamics simulations (11). Although the qualitative agreement with fluorescence and MD simulation is interesting, it should be realized that these two approaches each have their own limitations, and we believe that the NMR approach presented here is more accurate. In particular, the MD work is on a completely different timescale, and the motions seen by MD may or may not accurately reflect the population examined on the timescale of the NMR experiment. Our NMR analysis furthermore shows that both the tilt and rotation angles are very stable among the various subsets of constraints (Table 3, *lines A–E*). The wobbling and oscillation amplitudes are also determined with reasonable accuracy, although slightly less precisely than tilt and rotation. The oscillation amplitude, $\Delta\rho$, is very large (±84°), confirming that data analysis based on a semistatic, two-parameter model is inappropriate. The order of magnitude of $\Delta\rho$ is in complete agreement with the molecular dynamics simulation (11,50). It should be stressed that, compared with the GALA analysis, the rotation angle, ρ_0, initially determined is not modified. The angle of 155°, as determined in Ozdirekcan et al. (11,50) corresponds to 145° in the molecular frame used in this article, and hence corresponds well with the value of 146° obtained here. These results show that dynamical averaging mostly affects the tilt angle determination.
2. ^{15}N-^{13}C dipolar couplings obtained for this highly dynamic peptide are weak (~300 Hz). The accuracy is relatively low due to the low signal/noise ratio. Removal of these constraints does not significantly change the outcome of the fit (Table 3, *line B*), suggesting that one should proceed with the analysis without parameters from the fairly time-consuming REDOR experiments.
3. Adding ^{15}N-H dipolar couplings such as those that can be measured from the (also time-consuming) PISEMA

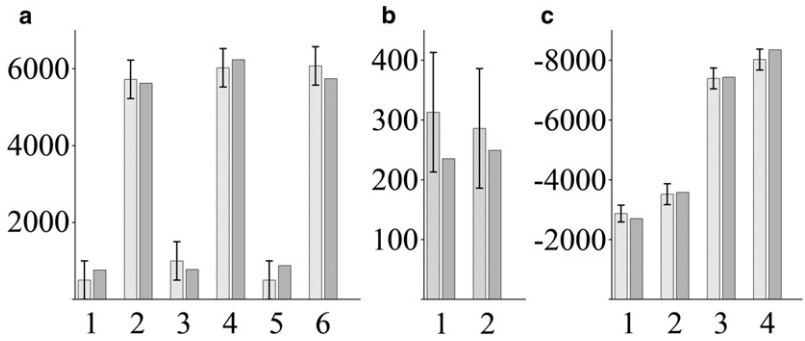

FIGURE 4 Best fit (*dark gray bars*) to the 12 experimental anisotropic constraints obtained from NMR (*light gray bars*) corresponding to results on line A of Table 1. (*a*) CD_3 quadrupolar couplings (Hz) of $Ala^{7,9,11,13,15,17}$ (1–6, respectively). (*b*) ^{15}N-$^{13}C_1$ dipolar couplings (Hz) of Ala^{11}-Leu^{12} (1) and Ala^{13}-Leu^{14} (2). (*c*) CSAs of $^{13}C_1$-Ala^{11} (1) and Ala^{13} (2) (Hz) and ^{15}N-Leu^{12} (3) and Leu^{14} (4) (Hz). The experimental values are summarized in Table 2.

experiment does not add much to the data analysis (Table 3, *line C*). This can be understood from the fact that the main tensor orientations of ^{15}N-H dipolar coupling and ^{15}N CSA interactions are similar, i.e., almost parallel to the helix axis. Both are very sensitive to the helix tilt (τ_0 and $\Delta\tau$) and less sensitive to helix rotation (ρ and $\Delta\rho$). Therefore, using only these two interactions is not sufficient for accurate data analysis (see Table 3, *line H*, where τ_0, $\Delta\tau$, and ρ_0 are different, and where $\Delta\rho$ is not determined), but using one of them is necessary (and sufficient) to separate the two pairs of variables. Accordingly, using only the six CD_3 quadrupolar splittings and two ^{15}N CSA values gives a good solution to the problem (Table 3, *line E*), whereas six quadrupolar splittings alone are not sufficient (Table 3, *lines F1* and *F2*; note that the best fitting in this case is obtained for F1, i.e., for a very small tilt angle). It should be stressed that the PISEMA experiment offers the advantage of a 2D experiment in terms of increased resolution, and thus makes it possible to obtain exploitable anisotropic interactions on uniformly ^{15}N-labeled peptides.

4. About exploring various motional models: largely similar conclusions were derived when a Gaussian distribution was used instead of a uniform distribution. In the case of the Gaussian distributions, a global minimum was found for $\tau_0 = 16.2° \pm 1.6°$, $\Delta\tau = 12.0° \pm 1.6°$, $\rho_0 = 146.6° \pm 15.4°$, $\Delta\rho = 98.2° \pm 5.5°$. Hence, a slightly smaller tilt angle was found, and the other parameters were well within the experimental error. Although MD simulations show that the helical structure is very stable (11,40,51), internal dynamics of the peptide is also expected to influence the data analysis to some extent. This point is currently under examination by assessing such ''internal order parameters'' from MD simulations and by incorporating them into the data fitting process.
5. In the search for an optimal strategy to do a dynamical analysis of a transmembrane peptide (with fast axial diffusion around the bilayer normal), we propose to use six anisotropic interactions that allow optimal sampling of different tensor orientations by selecting specific labeling positions along the peptide helix (Table 3, *line D*). Thus, accurate dynamical analysis is already possible by synthesizing only two different triply labeled peptides, each of which includes a ^2H (CD_3 on Ala_{11} or Ala_{13}), a $^{13}C_1$ (Ala_{11} or Ala_{13}) and a ^{15}N (Leu_{12} or Leu_{14}) label, which would require ~3–4 days of measurement time on a 500- to 700-MHz solid-state NMR spectrometer.
6. Regarding description of the motion in terms of order parameters: using the notation of Goormaghtigh et al. (52), one can convert the values of τ_0 and $\Delta\tau$ into values of order parameters. The distribution of helix axis can be described by the product of two order parameters: $S_{\text{helix}} = S_{\text{helix angle}} \times S_{\text{helix order}}$

TABLE 3 Best-fit parameters using various subsets of anisotropic NMR constraints and uniform distributions

	Number: nature of constraints	τ_0 (°) tilt	$\Delta\tau$ (°) wobbling	ρ_0 (°) rotation	$\Delta\rho$ (°) oscillation
A	12: complete ensemble (SSD = 0.36)	20.8 ± 1.4	12.2 ± 4.5	146 ± 7	84 ± 21
B	10: remove ^{15}N-^{13}C DC (SSD = 0.33)	21.0 ± 1.5	10.8 ± 6.3	146 ± 7	86 ± 19
C	14: adding two simulated ^{15}N-H DCs*	20.4 ± 1.8	11.3 ± 7.3	146 ± 6	82 ± 23
D	6: 2 ^{15}N CSA, 2 ^{13}C CSA, 2 CD_3 $\Delta\nu_Q$	21.9 ± 1.3	8.0 ± 6.5	149 ± 8	90 ± 20
E	8: 6 CD_3 + 2 ^{15}N CSA	21.2 ± 1.8	11.5 ± 5.5	147 ± 7	83 ± 28
F1	6: CD_3 $\Delta\nu_Q$ alone (sol a: SSD = 0.3)	2.8 ± 0.9	31.9 ± 1.7	147 ± 8	80 ± 21
F2	6: CD_3 $\Delta\nu_Q$ alone (sol b: SSD = 0.6)	21.2 ± 1.0	1.3 ± 1.3	146 ± 8	75 ± 36
H	4: 2 ^{15}N CSA + 2 ^{15}N-H DC	15.8 ± 1.6	23.9 ± 2.0	127 ± 109	30 ± 81

Every fit was performed using the data obtained at 33% hydration (water/(water + lipid + peptide), w/w). The fits result from uniform distributions (see comment 4 in numbered list in text for Gaussian distributions). The uncertainty of each parameter (3σ value) was computed by the Monte Carlo approach (36) as described in Materials and Methods.

*The simulated ^{15}N-H DCs were computed using the dynamical parameters obtained from solution A. SSD is the standard deviation.

$S_{\text{helix angle}} = < 3\cos^2(\tau_0) - 1 > /2$ is related to the average tilt angle, τ_0

$S_{\text{helix order}} = < 3\cos^2(\tau_1) - 1 > /2$ is related to the wobbling (brackets indicate the average over $\tau_1 \in [0,\Delta\tau]$) (see Supporting Material for angle definitions).

For the uniform distribution, the values $\tau_0 = 20.8^\circ$ and $\Delta\tau = 12.2^\circ$ translate into $S_{\text{helix angle}} = 0.81$, $S_{\text{helix order}} = 0.97$, and $S_{\text{helix}} = 0.78$. This value of $S_{\text{helix order}}$ is significantly higher than the molecular order parameter S_{zz} of a DPPC (53) or DMPC (54) lipid in the fluid phase, which is around 0.6. This is not surprising considering that the peptide is anchored on both sides of the bilayer, whereas the lipid molecules extend over only half of the bilayer.

Several methods have been used to study structural properties of membrane proteins and to determine tilt angle of transmembrane peptides, including solid-state NMR, EPR, CD, ATR-FTIR, and fluorescence spectroscopy (for a recent review, see Holt and Killian (55). All these techniques, like ^{2}H GALA NMR, are powerful and simple to interpret in terms of an averaged orientation of the helices (τ_0 and ρ_0). However, the existence of distributions of orientation (characterized by a wobbling, $\Delta\tau$, and oscillation, $\Delta\rho$, parameters) and averaging effects make things more difficult. For instance, it is clearly stated in the very comprehensive review of Goormaghtigh et al. (52) that in the usual data treatment of ATR infrared spectroscopy, "$S_{\text{helix order}}$ cannot be evaluated independently from $S_{\text{helix angle}}$", so that usually $S_{\text{helix order}}$ is set to 1 (i.e., $\Delta\tau = 0$). Moreover, in the case of WALP23, one has to deal with the existence of a nonaxially symmetric distribution of the rotation angle, ρ, and the associated amplitude of oscillations ($\Delta\rho$), and this had never been included in the data analysis for a tilted peptide, to the best of our knowledge.

CONCLUSIONS

In this work, we analyzed a data set of different NMR anisotropic interactions (quadrupolar couplings, dipolar couplings, and CSAs) with an extended, dynamical four-parameter (τ_0, $\Delta\tau$, ρ_0, $\Delta\rho$) peptide model. An averaged tilt angle of 21° for WALP23 peptides inserted into DMPC has been determined. This is much larger than the tilt angle of 5.2° obtained by ^{2}H GALA NMR analysis based on a quasistatic model and follows the trends toward larger tilt angles indicated from MD simulations. It also provides an accurate determination of rotation angle, wobbling, and oscillation amplitudes. It does not, however, give any indication of the various timescales of these motions. These could be obtained in principle by analyzing solid-state deuterium NMR inversion-recovery and Jeener-Broekaert relaxation data in a similar way to the one proposed by Prosser et al. for lipids (53) or for the peptide gramicidin (14). ^{1}H, ^{13}C, and ^{15}N relaxation studies in the rotation frame under magic-angle spinning and with static-oriented samples could also be used to characterize the motional model (56). It should be stressed, however, that for this particular case, the motional model should include at least three timescales, characterizing diffusion along the bilayer normal, wobbling, and oscillations (not counting slow ensemble motions of the bilayer).

In the strategy, the combination of at least three different anisotropic tensors possessing complementary orientations proved to be essential to solve the inherent under determination brought by the explicit introduction of dynamical averaging and to analyze the orientation and dynamics of transmembrane peptides in a precise and efficient way. This approach should be very generally applicable to any transmembrane peptide and will allow for assessment of the influence of hydrophobic mismatch not only on tilt angles but also on the amplitudes of wobbling and oscillations.

SUPPORTING MATERIAL

Additional text, references, and figure are available at http://www.biophysj.org/biophysj/supplemental/S0006-3495(10)00145-1.

The authors thank the CALcul en MIdi-Pyrénées (CALMIP) computing center for generous allocations of computer time, and Rutger Staffhorst, Jacques Doux, and Lucie Khemtémourian for peptide synthesis. The NMR spectra were recorded on spectrometers financed with the help of European Structural funds, Région Midi-Pyrénées, and CNRS.

We acknowledge financial support from the European Marie Curie program (A.H.) (BIOMEM, Contract MEST-CT 2004-007931) and Conseil Régional Midi-Pyrénées and PRES Université de Toulouse (L.R.).

REFERENCES

1. Hong, M. 2007. Structure, topology, and dynamics of membrane peptides and proteins from solid-state NMR spectroscopy. *J. Phys. Chem. B*. 111:10340–10351.
2. Nyholm, T. K. M., S. Özdirekcan, and J. A. Killian. 2007. How protein transmembrane segments sense the lipid environment. *Biochemistry*. 46:1457–1465.
3. Cross, T. A., and S. J. Opella. 1994. Solid-state NMR structural studies of peptides and proteins in membranes. *Curr. Opin. Struct. Biol.* 4:574–581.
4. Jones, D. H., K. R. Barber, …, C. W. Grant. 1998. Epidermal growth factor receptor transmembrane domain: 2H NMR implications for orientation and motion in a bilayer environment. *Biochemistry*. 37:16780–16787.
5. van der Wel, P. C. A., E. Strandberg, …, R. E. Koeppe 2nd. 2002. Geometry and intrinsic tilt of a tryptophan-anchored transmembrane α-helix determined by ^{2}H NMR. *Biophys. J.* 83:1479–1488.
6. Strandberg, E., S. Özdirekcan, …, J. A. Killian. 2004. Tilt angles of transmembrane model peptides in oriented and non-oriented lipid bilayers as determined by 2H solid-state NMR. *Biophys. J.* 86:3709–3721.
7. Vostrikov, V. V., C. V. Grant, …, R. E. Koeppe 2nd. 2008. Comparison of "Polarization inversion with spin exchange at magic angle" and "geometric analysis of labeled alanines" methods for transmembrane helix alignment. *J. Am. Chem. Soc.* 130:12584–12585.
8. de Planque, M. R. R., J. A. Kruijtzer, …, J. A. Killian. 1999. Different membrane anchoring positions of tryptophan and lysine in synthetic transmembrane α-helical peptides. *J. Biol. Chem.* 274:20839–20846.
9. de Planque, M. R. R., E. Goormaghtigh, …, J. A. Killian. 2001. Sensitivity of single membrane-spanning α-helical peptides to hydrophobic mismatch with a lipid bilayer: effects on backbone structure, orientation, and extent of membrane incorporation. *Biochemistry*. 40:5000–5010.
10. Esteban-Martín, S., and J. Salgado. 2007. The dynamic orientation of membrane-bound peptides: bridging simulations and experiments. *Biophys. J.* 93:4278–4288.

11. Özdirekcan, S., C. Etchebest, …, P. F. Fuchs. 2007. On the orientation of a designed transmembrane peptide: toward the right tilt angle? *J. Am. Chem. Soc.* 129:15174–15181.
12. Straus, S. K., W. R. Scott, and A. Watts. 2003. Assessing the effects of time and spatial averaging in 15N chemical shift/15N-1H dipolar correlation solid state NMR experiments. *J. Biomol. NMR.* 26:283–295.
13. Strandberg, E., S. Esteban-Martín, …, A. S. Ulrich. 2009. Orientation and dynamics of peptides in membranes calculated from 2H-NMR data. *Biophys. J.* 96:3223–3232.
14. Prosser, R. S., and J. H. Davis. 1994. Dynamics of an integral membrane peptide: a deuterium NMR relaxation study of gramicidin. *Biophys. J.* 66:1429–1440.
15. ten Kortenaar, P. B. W., B. G. Vandijk, …, G. I. Tesser. 1986. Rapid and efficient method for the preparation of Fmoc-amino acids starting from 9-fluorenylmethanol. *Int. J. Pept. Protein Res.* 27:398–400.
16. Gullion, T., and J. Schaefer. 1989. Rotational-echo double-resonance NMR. *J. Magn. Reson.* 81:196–200.
17. Gullion, T., and J. Schaefer. 1989. Detection of weak heteronuclear dipolar coupling by rotational-echo double-resonance nuclear magnetic resonance. *Adv. Magn. Reson.* 13:57–83.
18. Razdow, A. 1986. Mathcad. MathSoft, Needham, MA.
19. Gullion, T., D. B. Baker, and M. S. Conradi. 1990. New, compensated Carr-Purcell sequences. *J. Magn. Reson.* 89:479–484.
20. Frisch, M. J., …, J. A. Pople. 2004. Gaussian 03 Revision E.01, Gaussian, Inc., Wallingford, CT.
21. Maseras, F., and K. Morokuma. 1995. IMOMM a new integrated ab-initio plus molecular mechanics geometry optimization scheme of equilibrium structures and transition-states. *J. Comput. Chem.* 16:1170–1179.
22. Vreven, T., and K. Morokuma. 2000. On the application of the IMOMO (integrated molecular orbital plus molecular orbital) method. *J. Comput. Chem.* 21:1419–1432.
23. Becke, A. D. 1993. Density-functional thermochemistry. 3. The role of exact exchange. *J. Chem. Phys.* 98:5648–5652.
24. Lee, C., W. Yang, and R. G. Parr. 1988. Development of the Colle-Salvetti correlation-energy formula into a functional of the electron density. *Phys. Rev. B.* 37:785–789.
25. Foresman, A. E., and A. Frisch. 1996. Exploring Chemistry with Electronic Structure Methods, Second edition. Gaussian, Pittsburgh.
26. Dewar, M. J. S., M. L. McKee, and S. Rzepa. 1978. MNDO parameters for third-period elements. *J. Am. Chem. Soc.* 100:3607.
27. Dewar, M. J. S., and W. Thiel. 1977. MINDO/3 study of addition of singlet oxygen δ-G-1o-2 to 1,3-butadiene. *J. Am. Chem. Soc.* 99:2338–2339.
28. Anders, E., R. Koch, and P. Freunscht. 1993. Optimization and application of lithium parameters for PM3. *J. Comput. Chem.* 14:1301–1312.
29. Wolinski, K., and A. J. Sadlej. 1980. Self-consistent perturbation-theory: open-shell states in perturbation-dependent non-orthogonal basis-sets. *Mol. Phys.* 41:1419–1430.
30. Wolinski, K., J. F. Hinton, and P. Pulay. 1990. Efficient implementation of the gauge-independent atomic orbital method for NMR chemical-shift calculations. *J. Am. Chem. Soc.* 112:8251–8260.
31. Ditchfield, R. 1974. Self-consistent perturbation theory of diamagnetism I. A gauge-invariant LCAO method for NMR chemical shifts. *Mol. Phys.* 27:789–807.
32. McWeeny, R. 1962. Perturbation theory for the Fock-Dirac density matrix. *Phys. Rev.* 126:1028–1034.
33. London, F. J. 1937. Théorie quantique des courants interatomiques dans les combinaisons aromatiques. *J. Phys. Radium.* 8:397–409.
34. Schmidt-Rohr, K., and H. W. Spiess. 1994. Multidimensional solid-state NMR and polymers. Harcourt Brace, London. 444–452.
35. Czaplicki, J., G. Cornélissen, and F. F. Halberg. 2006. GOSA, a simulated annealing-based program for global optimization of nonlinear problems, also reveals transyears. *J. Appl. Biomed.* 4:87–94.
36. Bevington, P., and D. K. Robinson. 2003. Data Reduction and Error Analysis for the Physical Sciences. McGraw-Hill, New York. 212–216.
37. Hahn, T. 2005. CUBA: a library for multidimensional numerical integration. *Comput. Phys. Commun.* 168:78–95.
38. Killian, J. A., I. Salemink, …, D. V. Greathouse. 1996. Induction of nonbilayer structures in diacylphosphatidylcholine model membranes by transmembrane α-helical peptides: importance of hydrophobic mismatch and proposed role of tryptophans. *Biochemistry.* 35:1037–1045.
39. Daily, A. E., D. V. Greathouse, …, R. E. Koeppe 2nd. 2008. Helical distortion in tryptophan- and lysine-anchored membrane-spanning α-helices as a function of hydrophobic mismatch: a solid-state deuterium NMR investigation using the geometric analysis of labeled alanines method. *Biophys. J.* 94:480–491.
40. Ulmschneider, J. P., J. P. F. Doux, …, M. B. Ulmschneider. 2009. Peptide partitioning and folding into lipid bilayers. *J. Chem. Theory Comput.* 5:2202–2205.
41. Kol, M. A., A. N. C. van Laak, …, B. de Kruijff. 2003. Phospholipid flop induced by transmembrane peptides in model membranes is modulated by lipid composition. *Biochemistry.* 42:231–237.
42. Sparr, E., W. L. Ash, …, J. A. Killian. 2005. Self-association of transmembrane α-helices in model membranes: importance of helix orientation and role of hydrophobic mismatch. *J. Biol. Chem.* 280: 39324–39331.
43. Sparr, E., D. N. Ganchev, …, B. de Kruijff. 2005. Molecular organization in striated domains induced by transmembrane α-helical peptides in dipalmitoyl phosphatidylcholine bilayers. *Biochemistry.* 44:2–10.
44. Hartzell, C. J., M. Whitfield, …, G. P. Drobny. 1987. Determination of the N-15 and C-13 chemical-shift tensors of L–C-13 alanyl-L- N-15 alanine from the dipole-coupled powder patterns. *J. Am. Chem. Soc.* 109:5966–5969.
45. Marassi, F. M. 2002. NMR of peptides and proteins in oriented membranes. *Concepts Magn. Reson.* 14:212–224.
46. Wu, C. H., A. Ramamoorthy, …, S. J. Opella. 1995. Simultaneous characterization of the amide H-1 chemical shift,H-1-N-15 dipolar, and N-15 chemical-shift interaction tensors in a peptide bond by 3-dimensional solid-state NMR spectroscopy. *J. Am. Chem. Soc.* 117:6148–6149.
47. Cady, S. D., C. Goodman, …, M. Hong. 2007. Determining the orientation of uniaxially rotating membrane proteins using unoriented samples: a ^{2}H, ^{13}C, and ^{15}N solid-state NMR investigation of the dynamics and orientation of a transmembrane helical bundle. *J. Am. Chem. Soc.* 129:5719–5729.
48. Yamaguchi, S., D. Huster, …, M. Hong. 2001. Orientation and dynamics of an antimicrobial peptide in the lipid bilayer by solid-state NMR spectroscopy. *Biophys. J.* 81:2203–2214.
49. Holt, A., R. B. M. Koehorst, …, J. A. Killian. 2009. Tilt and rotation angles of a transmembrane model peptide as studied by fluorescence spectroscopy. *Biophys. J.* 97:2258–2266.
50. Özdirekcan, S., D. T. S. Rijkers, …, J. A. Killian. 2005. Influence of flanking residues on tilt and rotation angles of transmembrane peptides in lipid bilayers. A solid-state 2H NMR study. *Biochemistry.* 44:1004–1012.
51. Shi, L., A. Cembran, …, G. Veglia. 2009. Tilt and azimuthal angles of a transmembrane peptide: a comparison between molecular dynamics calculations and solid-state NMR data of sarcolipin in lipid membranes. *Biophys. J.* 96:3648–3662.
52. Goormaghtigh, E., V. Raussens, and J. M. Ruysschaert. 1999. Attenuated total reflection infrared spectroscopy of proteins and lipids in biological membranes. *Biochim. Biophys. Acta.* 1422:105–185.
53. Prosser, R. S., J. H. Davis, …, G. Kothe. 1992. Deuterium NMR relaxation studies of peptide-lipid interactions. *Biochemistry.* 31:9355–9363.
54. Mayer, C., G. Grobner, …, G. Kothe. 1990. Orientation-dependent deuteron spin-lattice relaxation times in bilayer membranes: characterization of the overall lipid motion. *Chem. Phys. Lett.* 165:155–161.
55. Holt, A., and J. A. Killian. 2010. Orientation and dynamics of transmembrane peptides: the power of simple models. *Eur. Biophys. J.* 39:209–621.
56. Fares, C., J. Qian, and J. H. Davis. 2005. Magic angle spinning and static oriented sample NMR studies of the relaxation in the rotating frame of membrane peptides. *J. Chem. Phys.* 122:194908.